

Attention at Rest Stays at Rest: Breaking Visual Inertia for Cognitive Hallucination Mitigation

Boyang Gong, Yu Zheng[†], Fanye Kong, Jie Zhou, and Jiwen Lu

Tsinghua University, Beijing, China
{gongby25, kongfy23}@mails.tsinghua.edu.cn, {yu-zheng, jzhou,
lujiwen}@tsinghua.edu.cn

Abstract. Like a body at rest that stays at rest, we find that visual attention in multimodal large language models (MLLMs) exhibits pronounced inertia, remaining largely static once settled during early decoding steps and failing to support the compositional understanding required for cognitive inference. While existing hallucination mitigation methods mainly target perceptual hallucinations concerning object existence or attributes, they remain inadequate for such cognitive hallucinations that require inter-object relational deduction. Through token-wise attention analysis, we identify this **visual inertia** as a key factor: attention to semantically critical regions remains persistently focused and fails to dynamically support relational inference. We thereby propose a training-free Inertia-aware Visual Excitation (IVE) method that breaks this inertial pattern by modeling cognitive inference as the dynamic responsiveness of visual attention. Specifically, IVE selects visual tokens that are dynamically emerging relative to historical attention trends while distinguishing tokens exhibiting inertial behavior. To further facilitate compositional inference, IVE introduces an inertia-aware penalty that discourages over-concentration and limits the persistence of attention within localized regions. Extensive experiments show that IVE is effective across various base MLLMs and multiple hallucination benchmarks, particularly for cognitive hallucinations. Code is available at <https://github.com/wfr429/IVE>.

Keywords: Cognitive Hallucination Mitigation · Attention Dynamics · Visual Inertia

1 Introduction

Driven by recent breakthroughs in Large Language Models (LLMs) [1, 13, 27, 64], Multimodal Large Language Models (MLLMs) [2, 22, 30, 31, 40, 42, 43, 65] have achieved remarkable advances in cross-modal content understanding and generation. By integrating multimodal information into coherent linguistic representations, MLLMs demonstrate impressive performance across various vision-language tasks [50, 52, 61, 62, 66]. Despite these advances, recent studies [9, 14, 25]

[†] Project Leader

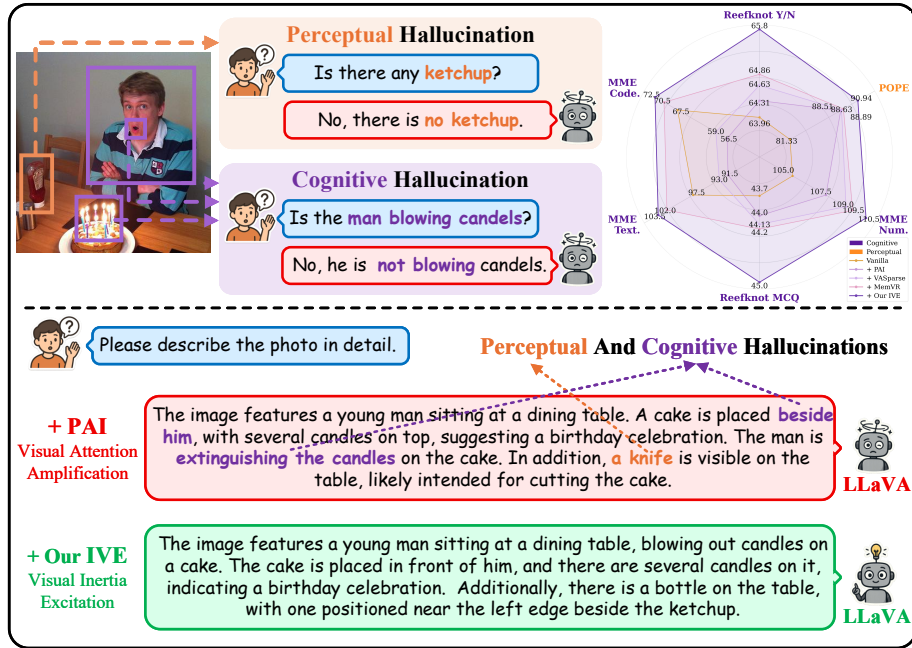


Fig. 1: Overview of the cognitive hallucinations and their mitigation via the proposed IVE. **Upper Left:** Comparison between perceptual and cognitive hallucinations in MLLMs. **Upper Right:** Comparison with hallucination mitigation methods across multiple benchmarks. **Bottom:** Compared to PAI [32] which amplifies visual attention designed primarily for mitigating perceptual hallucinations, our IVE effectively reduces both perceptual and cognitive hallucinations by exciting inertial visual attention.

have revealed that even advanced MLLMs may produce descriptions inconsistent with the provided images, a phenomenon known as MLLM hallucinations. This hallucination problem severely undermines MLLM reliability, limiting their practical applicability [3, 16, 29, 34, 46, 49].

To mitigate MLLM hallucinations, existing works can be broadly categorized into training-based and training-free methods. Training-based methods [20, 28, 39, 53, 54, 57] typically fine-tune models with instruction-response pairs or external supervision to enhance visual-linguistic alignment. In contrast, training-free methods [17, 19, 21, 45, 47, 55, 56, 67] focus on improving visual grounding without parameter updates. However, these methods predominantly address perceptual hallucinations concerning object existence or basic attributes. As recent evaluations [12, 33] have shown, cognition represents a higher-order capability built upon perception and is critical for reliable deployment in scenarios requiring relational inference [3, 34, 49]. Cognitive hallucinations, where models fabricate inter-object relationships even after correctly recognizing individual objects (Figure 1), are particularly difficult to detect through object-level verification, yet remain largely unaddressed by existing mitigation methods.

To develop targeted solutions, it is necessary to first understand what causes cognitive hallucinations internally. Prior work on perceptual hallucinations has

traced their origins to the model’s attention over visual tokens, finding that insufficient attention to task-relevant regions leads to fabricated objects [32, 51, 55]. A natural question arises: **do cognitive hallucinations share the same root cause?** We argue that they do not, because cognitive inference requires not merely attending to individual objects, but dynamically integrating cues across multiple regions to capture inter-object relationships. This motivates our analysis of attention during cognitive tasks (*cf.* Section 3), where we uncover a phenomenon we term **Visual Inertia**: as the model generates output, attention to key visual regions tends to remain persistently focused, failing to dynamically shift toward the compositional visual semantics required for relational inference. This finding also explains why naively amplifying visual attention [32] that is effective for perceptual hallucinations, yields diminishing returns for cognitive ones, as it reinforces static distributions rather than promoting the dynamic shifts that inference demands.

To address this limitation, we propose a training-free Inertia-aware Visual Excitation (IVE) method to mitigate cognitive hallucinations. Unlike previous methods that simply amplify attention, IVE explicitly breaks the inertial pattern of visual attention, reactivating it to emphasize overlooked visual regions that require compositional understanding of inter-object relationships. Specifically, we first identify visual tokens that dynamically emerge relative to historical attention trends while separating tokens exhibiting inertial behavior, enabling the model to focus on newly relevant regions. To further prevent persistent over-concentration on localized areas, IVE applies an Inertia-aware Attention Penalty that adaptively penalizes attention to tokens with sustained inertia, promoting the capture of compositional visual semantics necessary for relational inference. Extensive experiments demonstrate that IVE is effective across various baseline MLLMs [2, 8, 30] and multiple hallucination benchmarks [12, 25, 33, 63], showing particularly strong performance on cognitive hallucination tasks.

2 Related Works

Multimodal Large Language Models: Recently, Large Language Models (LLMs) have achieved remarkable breakthroughs in natural language understanding and generation [1, 13, 27, 64]. Building on these advances, Multimodal Large Language Models (MLLMs), developed for multimodal understanding and generation, have evolved from BERT-based decoders [10] to LLM-based architectures [40, 42, 43, 65], which significantly improve multimodal perception and understanding [50, 52, 61, 62, 66]. For example, LLaVA [31] and LLaVA-1.5 [30] achieve strong multimodal joint understanding by integrating pre-trained visual encoders with text decoders and incorporating instruction fine-tuning. BLIP-2 [22] and InstructBLIP [8] introduce the Q-Former mechanism to aggregate multimodal features, which improves the accuracy of cross-modal interactions. Qwen2.5-VL-Instruct [2] further improves cross-modal alignment via modular connections between vision and language models. In this work, we use widely-adopted MLLM baselines including LLaVA-1.5 [30], InstructBLIP [8],

and Qwen2.5-VL-Instruct [2], to evaluate the effectiveness of our proposed hallucination mitigation method.

Hallucination in MLLMs: Widely studied in LLMs [11, 23, 38, 60], hallucinations refer to inconsistencies between generated content and real-world facts or user instructions. Similar issues have also been observed in MLLMs [40, 42, 43], where generated descriptions may include inaccurate object details or conflict with the input image. To quantify such phenomena, many studies have proposed benchmarks for hallucination evaluation. CHAIR [37] and POPE [25] respectively evaluate object hallucinations and object-attribute accuracy. While most existing benchmarks focus on such low-level hallucinations on primitive visual perception, recent studies have extended to cognitive-level aspects. Reef-knot [63] addresses the evaluation of these cognitive hallucinations involving complex inter-object relationships, whereas MME [12] and MMBench [33] further benchmark MLLMs at the reasoning level. We systematically evaluate the effectiveness of our method in mitigating hallucinations on these benchmarks.

Hallucination Mitigation: Hallucination mitigation aims to make generated responses factually consistent with input text or visual content. In LLMs, researchers manipulate internal representations [23, 24, 59] to boost self-consistency across responses [36, 41]. For MLLMs, consistency requires non-conflicting semantics across modalities. Existing methods fall into two categories. Training-based approaches, like robust instruction tuning [18, 28, 53, 57] and reinforcement learning from human feedback (RLHF) [15, 20, 39, 54], use external supervision to reduce hallucinations at a high computational cost. Training-free methods mitigate perceptual hallucinations (object existence and attributes) by refining visual grounding during inference via early-layer features [17, 45] or perturbed inputs for contrastive decoding [4, 7, 21, 47]. While effective for perceptual-level hallucinations, cognitive-level hallucinations remain largely underexplored.

3 Preliminary and Motivation

3.1 Preliminary

Multimodal Large Language Models (MLLMs) typically consist of three core components: a visual encoder, a projector, and a large language model (LLM). Given a system prompt \mathcal{S} , a visual input \mathcal{V} (e.g., an image), and a user instruction \mathcal{I} , an MLLM generates a semantically consistent response \mathcal{Y} :

$$\mathcal{F} : (\mathcal{S}, \mathcal{V}, \mathcal{I}) \mapsto \mathcal{Y} \quad (1)$$

The pretrained visual encoder [5, 35, 58] and projector extract visual features and project them into text-aligned representations, enabling the LLM to generate contextually grounded responses in an autoregressive manner.

Tokens in MLLMs: MLLMs encode each modality into modality-specific token sequences, i.e., system tokens \mathbf{T}_s , visual tokens \mathbf{T}_v , and instruction tokens \mathbf{T}_i . These tokens are concatenated to form the input token sequence:

$$\mathbf{T} = [\mathbf{T}_s, \mathbf{T}_v, \mathbf{T}_i] \quad (2)$$

The interactions among these tokens are modeled through multi-head self-attention [44], which computes an attention matrix \mathbf{A} to capture contextual dependencies across modalities.

During autoregressive generation, each token is predicted conditioned on previously generated tokens and the input token sequence \mathbf{T} . Specifically, over N generated tokens:

$$P(\mathbf{Y} | \mathbf{T}) = \prod_{t=1}^N P(y_t | y_{<t}, \mathbf{T}) \quad (3)$$

3.2 Visual Inertia in Cognitive Hallucinations

Recent studies [32, 51, 55] have identified imbalanced token attention as a primary cause of perceptual hallucinations, where models fail to adequately attend to critical visual regions. Building on this finding, we conduct empirical analyses to investigate whether cognitive hallucinations exhibit similar attention patterns.

Our analysis reveals that, while cognitive hallucinations also show token attention imbalance, they exhibit an additional phenomenon referred to as **Visual Inertia**. To systematically assess it, we propose a metric that quantifies visual inertia. Attention to key visual regions exhibits pronounced visual inertia, gradually failing to dynamically shift toward the compositional semantics required for relational inference as generation progresses. This renders existing attention amplification methods [32] less effective for cognitive hallucinations.

Limited Effectiveness of Attention Amplification: To investigate whether amplifying attention to visual tokens \mathbf{T}_v mitigates cognitive hallucinations, we progressively increased the amplification factor following PAI [32]. As shown in Figure 2, mitigation of perceptual hallucinations on POPE [25] improves monotonically with stronger amplification. In contrast, cognitive hallucinations on Reefknot [63] show a non-monotonic pattern: performance first improves but declines when amplification is excessive. The observed performance degradation indicates that attention insufficiency alone does not fully explain cognitive hallucinations, and naive amplification fails to address the underlying cause.

Visual Inertia in Cognitive Hallucinations: Cognitive hallucinations generally occur in tasks that require relational inference involving multiple objects. Such inference necessitates the dynamic integration of cross-object relations essential for compositional understanding. We hypothesize that cognitive hallucinations originate from a distinct phenomenon, referred to as **Visual Inertia**,

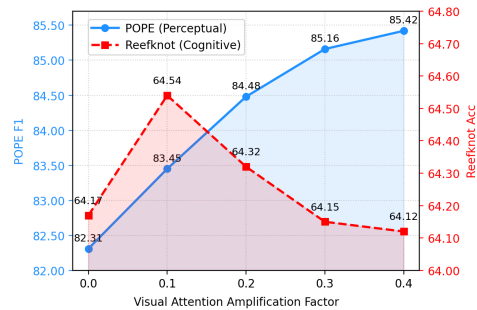


Fig. 2: Limited Effectiveness of Visual Attention Amplification on Cognitive Hallucinations. We assess the improvements of attention amplification (PAI) [32] on perceptual (POPE) [25] and cognitive (Reefknot) [63] hallucination benchmarks.

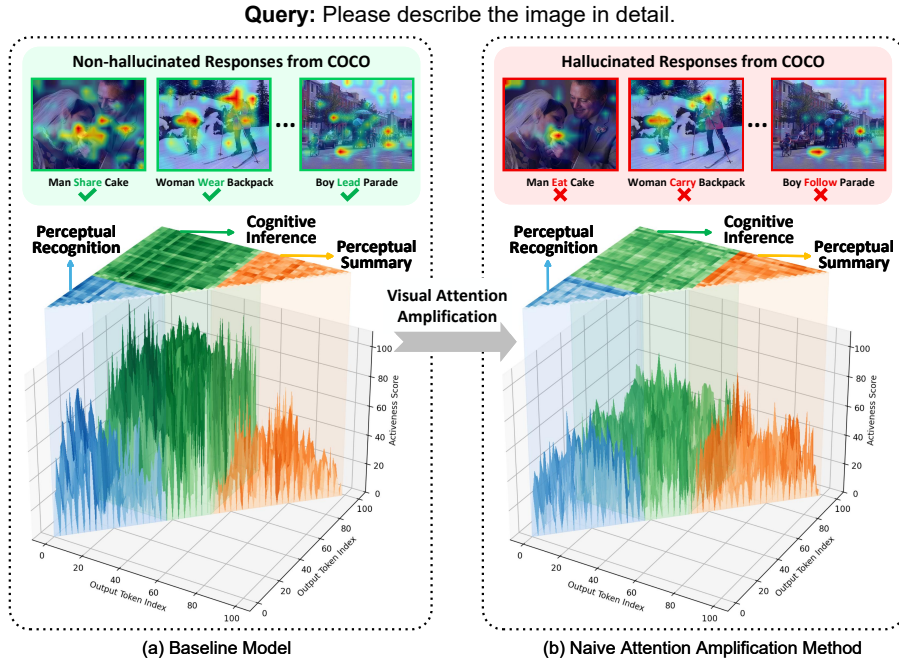


Fig. 3: The naive visual attention amplification method exacerbates visual inertia. A visual activeness comparison between (a) the baseline model and (b) the naive attention amplification method PAI [32] shows that the amplification strategy reduces visual attention activeness, thereby triggering cognitive hallucinations.

in which visual attention tends to remain concentrated within limited regions, thereby limiting the effective integration of cross-object relations. Under this hypothesis, increasing attention strength through amplification may inadvertently reduce attention activeness, which can hinder the process of integrating cross-object relations necessary for compositional inference.

Quantifying Visual Inertia: To investigate this hypothesis, we formalize visual attention activeness to measure visual inertia. We define visual activeness \mathcal{A} as the mean Wasserstein distance between consecutive output token attention distributions with the Manhattan distance on patch indices as the ground metric:

$$\mathcal{A} = \frac{1}{T-1} \sum_{i=1}^{T-1} W(\mathbf{p}_i, \mathbf{p}_{i+1}), \quad \text{where } \mathbf{p}_i = \frac{\sum_{h=1}^H \mathbf{A}_i^{(h)}}{\left\| \sum_{h=1}^H \mathbf{A}_i^{(h)} \right\|_1}. \quad (4)$$

Here, $\mathbf{A}_i^{(h)}$ denotes visual attention weights from the h -th head for the i -th output token, T is the total number of generated tokens, and $W(\cdot, \cdot)$ is the Wasserstein distance. Higher visual activeness \mathcal{A} indicates stronger attention switching between image regions during consecutive token generation.

Verification via Manual Inertia: To validate the effect of visual inertia on cognitive hallucinations, we applied a manual inertia procedure on LLaVA-

1.5 [30], updating attention at decoding step t as:

$$\mathbf{A}'_t = \mathbf{A}_t + \lambda \cdot \mathbf{A}_{t-1}, \quad (5)$$

where λ controls the induced inertia. The updated attention was re-normalized to maintain a valid distribution. Experiments on the Reefknot dataset [63] in Table 1 show that increasing visual inertia via step-wise propagation lowers visual activeness \mathcal{A} and response accuracy $\mathbf{R}_{\text{score}}$, which supports the hypothesis that visual inertia exacerbates cognitive hallucinations.

We generated 1,000 image descriptions using LLaVA-1.5 [30] on a subset of the COCO dataset [26]. For each description, we recorded the normalized visual attention weights for the first $T = 100$ output tokens and computed the corresponding pairwise Wasserstein distances as described above. Figure 3 presents a comparison between the base

Table 1: Visual inertia vs. cognitive hallucination.

λ	\mathcal{A}	$\mathbf{R}_{\text{score}} \uparrow$
0.0	41.52	63.96
0.5	27.68	54.87
1.0	19.24	47.25

model and a naive visual attention amplification method, PAI [32], during image captioning. The model with amplified attention consistently exhibits lower pairwise distances, indicating a reduction in the semantic activeness of visual attention. Notably, the naive visual attention amplification exacerbates visual inertia, preventing attention from dynamically shifting toward regions necessary for capturing compositional semantics required for relational inference, which contributes to the occurrence of cognitive hallucinations. Heatmaps in Figure 3 further illustrate that non-hallucinated responses distribute attention across multiple relationally relevant regions, whereas hallucinated responses remain confined to a limited spatial area.

4 Approach

In this section, we present the proposed Inertia-aware Visual Excitation (IVE) framework, as illustrated in Figure 4. Rather than heuristically manipulating attention weights, IVE is grounded in the insight that cognitive inference capability is closely related to the temporal dynamics of visual attention across decoding steps relative to historical attention trends, which requires breaking visual attention inertia to enable compositional understanding. We first introduce Trend-guided Token Selection, which identifies visual tokens that dynamically emerge relative to historical attention trends while separating tokens exhibiting inertial behavior, followed by Inertia-aware Attention Penalty, which penalizes persistent over-concentration on localized regions.

4.1 Trend-guided Token Selection

As shown in Section 3, MLLMs exhibit persistent visual inertia in key regions, limiting their capacity for cross-object relational inference. Attention-based methods [32, 51, 55] that amplify weights to increase visual focus can inadvertently reinforce this inertia. To address this, IVE leverages historical attention trends to partition visual tokens into two categories (top right of Figure 4):

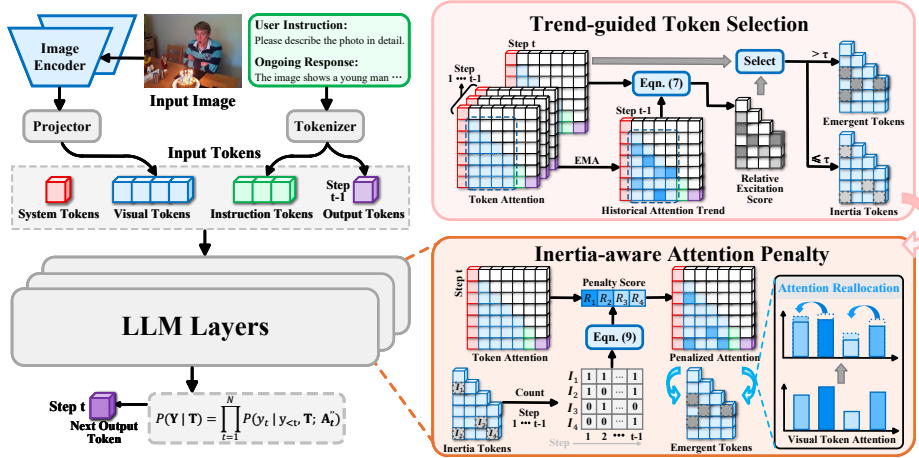


Fig. 4: Overview of our proposed IVE framework. **Left:** The autoregressive generation process of MLLMs integrated with IVE, which operates on token attention during next-token prediction. **Top Right:** Trend-guided Token Selection partitions visual tokens according to their temporal deviation from historical attention trends, distinguishing dynamically emergent tokens from inertia tokens that maintain stable concentration patterns, thereby enabling adaptive emphasis on newly relevant visual regions. **Bottom Right:** Inertia-aware Attention Penalty quantifies the persistence of inertia tokens across decoding steps and progressively attenuates their influence, reallocating the penalized attention toward emergent tokens to discourage prolonged over-concentration on historically dominant regions.

emergent tokens, which become newly prominent or dynamically active relative to historical patterns, and inertia tokens, which persistently over-concentrate on historically dominant regions, thereby enabling more effective integration of newly relevant visual cues into cognitive inference.

Identifying these tokens requires modeling accumulated attention trajectories rather than relying on instantaneous attention values. Let $\mathbf{A}_t^{(h)} \in \mathbb{R}^N$ denote the attention vector from the current query token to all tokens at decoding step t in head h , where N is the number of tokens. The attention weight assigned to token j at step t is the average attention across all heads:

$$a_{t,j} = \frac{1}{H} \sum_{h=1}^H \mathbf{A}_{t,j}^{(h)}, \quad (6)$$

where $\mathbf{A}_{t,j}^{(h)}$ denotes the attention weight from the current query token to token j in head h , and H is the number of attention heads.

A single-step distribution cannot reveal whether a token exhibits genuine temporal activity or simply maintains a persistent concentration pattern. To capture temporal behavior, an Exponential Moving Average (EMA) tracks the historical evolution of attention weights, allowing the current value to be compared against its smoothed historical reference. Specifically, the EMA is updated

up to step $(t - 1)$ as:

$$\tilde{a}_{t-1,j} = \gamma \cdot \tilde{a}_{t-2,j} + (1 - \gamma) \cdot a_{t-1,j}, \quad (7)$$

where $\gamma \in (0, 1)$ controls the degree of temporal smoothing. Here, $\tilde{a}_{t-1,j}$ represents the EMA-smoothed attention weight for token j . Based on historical attention trends, the relative excitation score for token j at step t is defined as:

$$S_{t,j} = \frac{a_{t,j} - \tilde{a}_{t-1,j}}{\sqrt{\tilde{a}_{t-1,j}(1 - \tilde{a}_{t-1,j})} + \epsilon}, \quad (8)$$

where $\epsilon = 10^{-6}$ ensures numerical stability. This scales the deviation by the magnitude of historical attention, allowing consistent comparison across tokens. Consequently, tokens with substantial attention growth relative to the historical baseline obtain higher excitation scores, highlighting emergent visual regions while suppressing persistently dominant tokens caused by visual inertia.

Token selection is performed using a threshold τ for emergent tokens, while inertia tokens are identified by their historical average attention:

$$\mathcal{E}_t = \{j \mid S_{t,j} > \tau\}, \quad \mathcal{I}_t = \{j \mid \bar{a}_{t-1,j} > \tau \text{ and } S_{t,j} \leq \tau\}, \quad (9)$$

where $\bar{a}_{t-1,j}$ is the average attention of token j up to step $(t - 1)$. \mathcal{E}_t contains emergent tokens showing notable temporal activity when generating the current text token, supporting cross-object interactions for relational inference. \mathcal{I}_t includes inertia tokens maintaining persistent attention over time.

4.2 Inertia-aware Attention Penalty

While selecting dynamically emerging tokens aids the integration of visual cues into compositional inference, attention can remain concentrated on historically dominant regions across decoding steps. Such sustained focus limits the model’s capacity to capture cross-object relational semantics for cognitive inference. To address this, Inertia-aware Attention Penalty (bottom right of Figure 4) adaptively penalizes tokens exhibiting inertial behavior.

The persistence of each inertial token is quantified by accumulating its historical selections:

$$C_{t,j} = \sum_{k=1}^{t-1} \mathbf{1}(j \in \mathcal{I}_k), \quad (10)$$

where $\mathbf{1}(\cdot)$ is 1 if token j is selected at step k , and 0 otherwise. This counts the preceding decoding steps in which token j was categorized as inertial.

Directly penalizing frequently selected tokens may reduce sensitivity to essential visual cues. To balance penalization with effective grounding, the attention of inertial tokens is attenuated proportionally to their historical inertia:

$$a'_{t,j} = a_{t,j} \left(1 - \alpha \frac{C_{t,j}}{t-1} \right), \quad j \in \mathcal{I}_t, \quad (11)$$

where $\alpha > 0$ controls the penalty intensity, gradually reducing the influence of persistently inertial tokens while preserving informative signals. The total penalized attention is:

$$R_t = \sum_{j \in \mathcal{I}_t} (a_{t,j} - a'_{t,j}). \quad (12)$$

Instead of simple redistribution, the penalized attention is reallocated to emergent tokens in \mathcal{E}_t proportionally to their relative deviation scores:

$$w_{t,j} = \frac{S_{t,j}}{\sum_{k \in \mathcal{E}_t} S_{t,k}}, \quad j \in \mathcal{E}_t, \quad (13)$$

and the updated attention distribution is:

$$a''_{t,j} = \begin{cases} a'_{t,j} + w_{t,j}R_t, & j \in \mathcal{E}_t, \\ a'_{t,j}, & \text{otherwise.} \end{cases} \quad (14)$$

This mechanism suppresses inertia-driven tokens while enhancing dynamically emerging ones, ensuring attention is adaptively focused on relevant regions. Attention reallocation is applied across all layers on per-token attention aggregated over all heads, without modifying individual heads separately.

During generation, inertia-aware modulation is applied to the attention matrix before computing the next-token distribution, as shown in the left part of Figure 4. Specifically, the redistributed attention $\mathbf{A}''_t = \{a''_{t,j}\}$ replaces the original \mathbf{A}_t at each step:

$$P(\mathbf{Y} | \mathbf{T}) = \prod_{t=1}^N P(y_t | y_{<t}, \mathbf{T}; \mathbf{A}''_t). \quad (15)$$

By conditioning decoding on the regulated attention at every step, excessive reliance on repetitive regions is mitigated, improving compositional inference and reducing cognitive hallucinations.

5 Experiments

In this section, we evaluate IVE through extensive experiments. Unlike existing methods that mainly focus on perceptual hallucinations concerning object existence or attributes, IVE is designed to mitigate cognitive hallucinations that require inter-object relational inference. We perform comprehensive comparisons across various base MLLMs and multiple hallucination and performance benchmarks. In addition, we conducted ablation studies to evaluate the impact of hyperparameters and the computational efficiency of our method.

5.1 Experimental Settings

Benchmarks: We conduct a comprehensive evaluation of IVE across three MLLM benchmark categories. (i) Reefknot [63] and MME [12] assess complex

Table 2: Cognitive Hallucination Mitigation on MME Benchmark [12]. Results on the cognitive subset of MME benchmark across three MLLMs. Com., Num., Text., and Code denote commonsense reasoning, numerical calculation, text translation, and code reasoning respectively.

Method	LLaVA-1.5 [30]				InstructBLIP [8]				Qwen2.5-VL-Instruct [2]			
	Com.↑	Num.↑	Text.↑	Code.↑	Com.↑	Num.↑	Text.↑	Code.↑	Com.↑	Num.↑	Text.↑	Code.↑
Vanilla	88.00	105.0	97.50	67.50	118.0	40.00	92.50	55.00	73.00	95.00	185.0	140.0
+VCD [21]	90.50	101.0	98.50	65.00	119.0	45.50	94.50	57.50	74.50	98.50	182.5	142.0
+OPERA [17]	93.00	108.5	92.50	57.50	122.5	48.00	89.50	52.00	78.00	100.5	177.5	138.5
+PAI [32]	92.00	107.5	91.50	56.50	121.5	47.50	89.00	51.50	77.00	100.0	176.5	137.5
+Deco [45]	91.50	102.5	100.0	70.00	121.0	46.50	96.00	59.50	75.50	98.50	187.5	144.5
+VASparse [67]	93.50	109.0	93.00	59.00	122.0	48.50	91.00	53.50	77.50	101.0	180.0	140.0
+MemVR [68]	94.50	109.5	102.0	70.50	123.0	48.00	97.50	60.00	78.00	101.5	187.0	145.0
+Ours	95.50	110.5	103.5	72.50	124.5	49.50	98.50	61.50	79.50	103.5	188.5	146.5
Improvement	+7.50	+5.50	+6.00	+5.00	+6.50	+9.50	+6.00	+6.50	+6.50	+8.50	+3.50	+6.50

Table 3: Cognitive Hallucination Mitigation on Reefknot benchmark [63]. Results (%) of various decoding strategies across three MLLMs. Perc./Cogn. denote perception/cognition hallucination rates, and R_{score} measures response accuracy.

Category	Method	LLaVA-1.5 [30]			InstructBLIP [8]			Qwen2.5-VL-Instruct [2]		
		Perc.↓	Cogn.↓	R_{score} ↑	Perc.↓	Cogn.↓	R_{score} ↑	Perc.↓	Cogn.↓	R_{score} ↑
Y/N	Vanilla	37.67	33.99	63.96	45.31	42.47	55.94	37.22	20.58	70.12
	+VCD [21]	37.33	33.67	64.58	45.22	42.35	56.05	37.13	20.47	70.23
	+OPERA [17]	37.08	33.23	64.62	45.03	42.05	56.28	36.86	20.12	70.53
	+PAI [32]	37.21	33.77	64.31	44.89	41.86	56.45	36.82	19.95	70.63
	+Deco [45]	37.22	33.42	64.51	45.17	42.21	56.14	37.00	20.33	70.36
	+VASparse [67]	37.13	33.14	64.63	44.67	42.47	56.30	36.91	20.86	70.17
	+MemVR [68]	36.99	32.81	64.86	44.34	42.09	56.65	36.75	20.16	70.57
	+Ours	35.88	32.07	65.80	43.75	40.60	57.64	35.97	18.93	71.55
	Improvement	-1.79	-1.92	+1.84	-1.56	-1.87	+1.70	-1.25	-1.65	+1.43
MCQ	Vanilla	68.05	51.04	43.70	73.91	53.85	39.94	67.16	49.69	44.91
	+VCD [21]	67.86	50.90	43.86	73.67	53.75	40.09	67.02	49.58	45.02
	+OPERA [17]	67.12	50.21	44.56	72.98	53.23	40.66	66.51	49.13	45.50
	+PAI [32]	66.93	51.10	44.00	74.05	53.83	39.91	67.58	49.25	45.08
	+Deco [45]	67.54	50.73	44.07	73.30	53.60	40.30	66.84	49.38	45.22
	+VASparse [67]	67.21	50.88	44.13	73.91	53.48	40.20	66.51	49.21	45.44
	+MemVR [68]	66.98	50.79	44.20	73.40	53.19	40.56	66.37	49.15	45.53
	+Ours	66.19	50.00	45.00	72.09	52.19	41.66	65.72	48.33	46.29
	Improvement	-1.86	-1.04	+1.30	-1.82	-1.66	+1.72	-1.44	-1.36	+1.38

inter-object relations as indicators of cognitive hallucinations. (ii) POPE [25] evaluates perceptual hallucinations, including object misidentification and object-attribute consistency. (iii) MMBench [33] provides a multidimensional assessment of MLLM performance across perception, cognition, and reasoning.

Models: We evaluate our method on three representative MLLMs: LLaVA-1.5 [30], InstructBLIP [8], and Qwen2.5-VL-Instruct [2]. All models use large-scale pretrained vision encoders, such as CLIP [35], paired with pretrained language models, including LLaMA [42] or Vicuna [6]. For consistency, all models used in our experiments have 7B parameters, and detailed prompt templates for each benchmark are provided in the appendix.

Baselines: We compare IVE with several state-of-the-art hallucination mitigation methods, including VCD [21], OPERA [17], Deco [45], PAI [32], VASparse [67] and MemVR [68], all evaluated under a unified beam search decoding

Table 4: Perceptual Hallucination Mitigation on POPE benchmark [25]. Accuracy and F1-score (%) comparison under different evaluation settings (i.e., Random, Popular and Adversarial). Δ denotes improvement over vanilla baseline.

Category	Method	LLaVA-1.5 [30]				InstructBLIP [8]				Qwen2.5-VL-Instruct [2]			
		Acc \uparrow	Δ	F1 \uparrow	Δ	Acc \uparrow	Δ	F1 \uparrow	Δ	Acc \uparrow	Δ	F1 \uparrow	Δ
Random	Vanilla	83.29	+0.00	81.33	+0.00	80.71	+0.00	80.41	+0.00	85.27	+0.00	85.30	+0.00
	+VCD [21]	86.27	+2.98	86.34	+5.01	84.53	+3.82	83.68	+3.27	88.60	+3.33	88.67	+3.37
	+OPERA [17]	88.30	+5.01	88.36	+7.03	85.80	+5.09	85.89	+5.48	89.87	+4.60	89.93	+4.63
	+Deco [45]	88.13	+4.84	88.20	+6.87	84.87	+4.16	84.79	+4.38	89.63	+4.36	89.68	+4.38
	+PAI [32]	88.42	+5.13	88.51	+7.18	85.20	+4.49	85.29	+4.88	89.77	+4.50	89.82	+4.52
	+VASparse [67]	88.57	+5.28	88.63	+7.30	86.20	+5.49	86.28	+5.87	89.97	+4.70	90.02	+4.72
	+MemVR [68]	88.83	+5.54	88.89	+7.56	86.57	+5.86	86.64	+6.23	90.40	+5.13	90.45	+5.15
	+Ours	90.53	+7.24	90.94	+9.61	90.20	+9.49	90.16	+9.75	92.10	+6.83	92.15	+6.85
	Popular	Vanilla	81.88	+0.00	80.06	+0.00	78.22	+0.00	78.36	+0.00	83.73	+0.00	83.83
+VCD [21]		83.67	+1.79	83.77	+3.71	80.70	+2.48	80.80	+2.44	85.03	+1.30	85.12	+1.29
+OPERA [17]		84.60	+2.72	84.69	+4.63	81.97	+3.75	82.07	+3.71	86.33	+2.60	86.41	+2.58
+Deco [45]		83.90	+2.02	83.99	+3.93	81.33	+3.11	81.44	+3.08	85.47	+1.74	85.54	+1.71
+PAI [32]		84.13	+2.25	84.23	+4.17	81.60	+3.38	81.71	+3.35	85.91	+2.18	85.98	+2.15
+VASparse [67]		84.77	+2.89	84.84	+4.78	82.17	+3.95	82.27	+3.91	86.57	+2.84	86.64	+2.81
+MemVR [68]		85.00	+3.12	85.09	+5.03	82.50	+4.28	82.60	+4.24	86.83	+3.10	86.91	+3.08
+Ours		86.90	+5.02	87.01	+6.95	84.73	+6.51	85.45	+7.09	89.70	+5.97	89.75	+5.92
Adversarial	Vanilla	76.47	+0.00	76.61	+0.00	74.37	+0.00	74.51	+0.00	81.87	+0.00	81.98	+0.00
	+VCD [21]	77.20	+0.73	77.34	+0.73	76.80	+2.43	76.94	+2.43	83.47	+1.60	83.57	+1.59
	+OPERA [17]	78.00	+1.53	78.13	+1.52	77.50	+3.13	77.63	+3.12	84.67	+2.80	84.76	+2.78
	+Deco [45]	77.57	+1.10	77.68	+1.07	77.07	+2.70	77.21	+2.70	83.87	+2.00	83.97	+1.99
	+PAI [32]	77.83	+1.36	77.96	+1.35	77.37	+3.00	77.49	+2.98	84.30	+2.43	84.39	+2.41
	+VASparse [67]	78.30	+1.83	78.42	+1.81	78.13	+3.76	78.53	+4.02	84.87	+3.00	84.93	+2.95
	+MemVR [68]	78.60	+2.13	78.73	+2.12	78.40	+4.03	78.42	+3.91	85.47	+3.60	85.56	+3.58
	+Ours	80.53	+4.06	82.17	+5.56	80.50	+6.13	81.70	+7.19	88.17	+6.30	88.23	+6.25

framework. For fair comparison, all methods are implemented using the default hyperparameters from their official repositories.

Implementation Details: We implement IVE using HuggingFace Transformers [48] and integrate it with beam search for decoding. All experiments are conducted on 8 NVIDIA H800 GPUs. The EMA smoothing coefficient γ is fixed at 0.1, and the selection threshold τ is set to 3.0. The penalty score α is tuned for each model and benchmark. Additional implementation details and experimental results are provided in the appendix.

5.2 Main Results

Cognitive Hallucination: We evaluated the effectiveness of our method IVE in mitigating cognitive hallucinations on two benchmarks [12, 63]. As shown in Table 3, it outperforms existing approaches on the two tasks in Reefknot [63] evaluated across three models. Compared to methods designed for perceptual hallucinations [17, 21, 45], IVE improves performance by up to 1.92% on

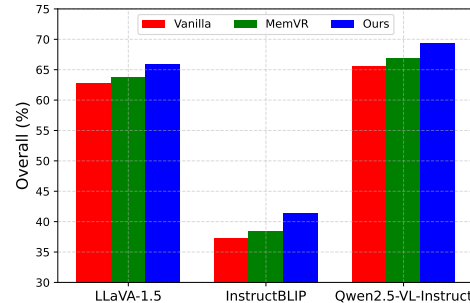


Fig. 5: Results (%) on the MMBench [33] benchmark, which assesses the multidimensional performance of MLLMs.

Table 5: Comparison of inference latency and computational cost across various decoding strategies on the Reefknot benchmark [63].

Model	Method	Perc.↓	Cogn.↓	R _{score} ↑	Time↓	Memory↓
LLaVA-1.5 [30]	Vanilla	37.67	33.99	63.96	0:14:44	15.15 G
	+VCD [21]	37.33	33.67	64.58	0:38:23	16.06 G
	+OPERA [17]	37.08	33.23	64.62	0:17:51	15.72 G
	+MemVR [68]	36.99	32.81	64.86	0:16:07	15.54 G
	+Ours	35.88	32.07	65.80	0:15:47	15.38 G
InstructBLIP [8]	Vanilla	45.31	42.47	55.94	0:47:02	31.13 G
	+VCD [21]	45.22	42.35	56.05	1:50:08	32.17 G
	+OPERA [17]	45.03	42.05	56.28	0:56:23	31.79 G
	+MemVR [68]	44.34	42.09	56.65	0:53:25	31.68 G
	+Ours	43.75	40.60	57.64	0:52:52	31.45 G
Qwen2.5-VL-Instruct [2]	Vanilla	37.22	20.58	70.12	0:31:46	33.41 G
	+VCD [21]	37.13	20.47	70.23	1:32:21	34.65 G
	+OPERA [17]	36.86	20.12	70.53	0:36:52	33.95 G
	+MemVR [68]	36.75	20.16	70.75	0:34:02	33.72 G
	+Ours	35.97	18.93	71.55	0:33:45	33.61 G

cognitive hallucination tasks, surpassing the state-of-the-art MemVR [68], which achieves only 0.68%. We further evaluated IVE on the MME [12] benchmark for cognitive hallucinations. As shown in Table 2, it outperforms existing approaches across a range of cognition tasks.

Perceptual Hallucination: Given its effectiveness in mitigating cognitive hallucinations, we further evaluated our method on perceptual hallucinations. As shown in Table 4, it achieves the best performance on the POPE benchmark [25], which targets object existence and attributes. Across different backbone models, our method consistently outperforms alternatives, and the largest gains in the POPE random setting are 9.61%, 9.75%, and 6.85%. These results indicate that our method is also effective in reducing perceptual hallucinations.

Multidimensional Performance of MLLMs: As shown in Figure 5, IVE consistently outperforms the state-of-the-art method MemVR [68] on the MM-Bench dataset [33], demonstrating superior performance across perception, cognition, and reasoning tasks.

5.3 Ablation Studies and Analysis

In this subsection, we present ablation studies to evaluate the contributions of the hyperparameters and the computational efficiency of the model. Further results and analysis are provided in the appendix.

Table 6: Ablation study on key coefficient of IVE.

Model	α	Reefknot [63]			POPE [25]	
		Perc.↓	Cogn.↓	R _{score} ↑	Acc↑	F1↑
LLaVA-1.5 [30]	0.05	36.84	32.72	65.46	89.20	89.27
	0.10	35.88	32.07	65.80	90.53	90.94
	0.15	36.60	32.43	65.73	89.57	89.62
InstructBLIP [8]	0.05	44.28	41.73	57.15	87.23	87.31
	0.10	43.75	40.60	57.64	90.20	90.16
	0.15	43.88	41.34	57.54	88.93	88.95

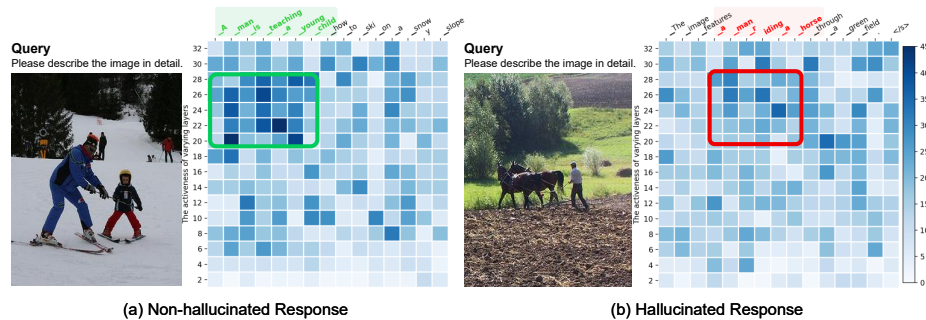


Fig. 6: Visualization of visual activeness of each token, comparing hallucinated and non-hallucinated responses in cognitive hallucination tasks. Rows indicate layer indices in LLaVA-1.5 [30], and columns correspond to decoded tokens at each step.

both LLaVA-1.5 [30] and InstructBLIP [8] achieve strong performance on Reefknot [63] and POPE [25] benchmarks, reducing cognitive and perceptual hallucinations. Notably, all tested hyperparameter configurations surpass the state-of-the-art method MemVR [68], demonstrating the robustness and generalizability of IVE.

Analysis of Inference Latency and Computational Cost: As shown in Table 5, we compare inference latency, GPU memory usage, and hallucination performance across decoding strategies on the Reefknot [63] benchmark. Across three backbones, the proposed method achieves the best overall performance with marginal overhead, attaining R_{score} values of 65.80%, 57.64%, and 71.55% on LLaVA-1.5 [30], InstructBLIP [8], and Qwen2.5-VL-Instruct [2], respectively, together with the lowest perceptual and cognitive hallucination rates. Compared with VCD [21], OPERA [17] and MemVR [68], it provides higher accuracy with less inference time and comparable or lower memory consumption.

Visualization of Visual Activeness: As shown in Figure 6, visual activeness varies dynamically across different layers during generation. Green-outlined regions indicate higher visual activeness in layers 20–28 when the MLLM analyzes inter-object cognitive relationships. Red-outlined regions indicate lower visual activeness for hallucinatory tokens such as `_r`, `iding`, `_a`, demonstrating that the proposed metric effectively captures the activeness of visual information.

6 Conclusion

In this paper, we propose Inertia-aware Visual Excitation (IVE) method to mitigate cognitive hallucinations. Unlike existing methods that mainly target perceptual hallucinations concerning object existence or attributes, IVE explicitly models cognitive inference as the dynamic responsiveness of visual attention. Inspired by the observation that attention to visual tokens often exhibits persistent inertia, IVE identifies visual tokens that emerge relative to historical attention trends while distinguishing tokens exhibiting inertial behavior, enabling adap-

tive attention reallocation. To further mitigate persistent attention on inertia tokens and promote compositional inference, IVE introduces an inertia-aware penalty that discourages over-concentration and constrains persistent attention within localized regions. Extensive experiments demonstrate that IVE is effective across various base MLLMs and multiple hallucination benchmarks, with particular success in addressing cognitive hallucinations.

Appendix

Section 1. Prompt Templates for Datasets.

- § Prompt Templates for Reefknot Dataset.
- § Prompt Templates for MME Dataset.
- § Prompt Templates for POPE Dataset.
- § Prompt Templates for MMBench Dataset.

Section 2. More Experimental Results and Analysis.

- § Radar Chart Results on InstructBLIP and Qwen2.5-VL-Instruct in Addition to LLaVA-1.5.
- § Heatmap Comparison Between our IVE and PAI.
- § Visual Activeness Comparison Between our IVE and PAI.
- § Ablation Study on Key Coefficients γ and τ .

Section 3. Case Studies Across Different Datasets.

- § Case Study on Reefknot Dataset.
- § Case Study on MME Dataset.
- § Case Study on POPE Dataset.
- § Case Study on MMBench Dataset.

7 Prompt Templates for Datasets

Prompt Templates for Reefknot Dataset: The Reefknot dataset [63] is specifically designed to evaluate cognitive hallucinations that arise from complex inter-object relationships in visual scenes, which often require models to perform relational reasoning beyond simple visual recognition and object detection. In the Reefknot dataset [63], the input template for the model is presented below, where the prompts are highlighted in **green** and the image is highlighted in **red** for clearer illustration of the input structure and the interaction format provided to the model during evaluation.

A chat between a curious user and an artificial intelligence assistant. The assistant gives helpful, detailed, and polite answers to the user’s questions.

USER: IMAGE

(i) Y/N:

Is the dog smelling frisbee in this photo? Please answer yes or no.

(ii) Multichoice:

What is the relation with sign and building in this photo?

A. into B. over C. towards D. within

Please choose.

ASSISTANT:

Prompt Templates for POPE Dataset: The POPE dataset [25] is specifically designed to evaluate object hallucinations and object–attribute consistency within perceptual hallucinations in MLLMs. In the POPE dataset [25], the input template for the model is presented below, where the prompts are highlighted in **green** and the image is highlighted in **red** for clearer visualization.

A chat between a curious user and an artificial intelligence assistant. The assistant gives helpful, detailed, and polite answers to the user’s questions.

USER: IMAGE

(i) Existence:

Is there a snowboard in the image? Please just answer yes or no.

(ii) Attribute:

Is the snowboard in the image red? Please just answer yes or no.

ASSISTANT:

Prompt Templates for MME Dataset: The MME dataset [12] provides a comprehensive benchmark for systematically evaluating various capabilities of MLLMs. Here, we specifically focus on the subsets related to cognitive hallucinations. We select the cognitive and reasoning-oriented tasks from MME [12], including commonsense reasoning, numerical calculation, text translation, and code reasoning, which are particularly prone to cognitive hallucinations. In the MME dataset [12], the input template for the model is presented below, where the prompts are highlighted in **green** and the image is highlighted in **red** for clearer illustration.

A chat between a curious user and an artificial intelligence assistant. The assistant gives helpful, detailed, and polite answers to the user’s questions.

USER: IMAGE

The image shows a python code. Is the output of the code “36”?

ASSISTANT:

Prompt Templates for MMBench Dataset: The MMBench dataset [33] provides a multidimensional and comprehensive assessment of MLLM performance across perception, cognition, and reasoning capabilities. In the MMBench dataset [33], the input template for the model is presented below, where the prompts are highlighted in **green** and the image is highlighted in **red** for clearer presentation.

A chat between a curious user and an artificial intelligence assistant. The assistant gives helpful, detailed, and polite answers to the user’s questions.

USER: IMAGE

Which one describes capybaras?

- A. Shy animals that hide in tall grass.
- B. Wild guinea pigs that live in mountain.
- C. Closest relatives of the hippopotamus.
- D. Large rodents that are good swimmers.

Please choose.

ASSISTANT:

8 More Experimental Results and Analysis

Radar Chart Results on InstructBLIP and Qwen2.5-VL-Instruct in Addition to LLaVA-1.5: Figure 7 presents a systematic comparison with hallucination mitigation methods across multiple benchmarks under two additional models, *i.e.*, InstructBLIP [8] and Qwen2.5-VL-Instruct [2]. Notably, the results consistently indicate that IVE achieves superior performance compared with other methods under both base models, demonstrating strong effectiveness and robustness across diverse evaluation settings. This superior performance is particularly evident on benchmarks targeting cognitive hallucinations, such as Reefknot [63] and MME [12], as well as on perceptual hallucination benchmarks like POPE [25], where IVE outperforms competing methods by a clear margin across multiple tasks and evaluation criteria.

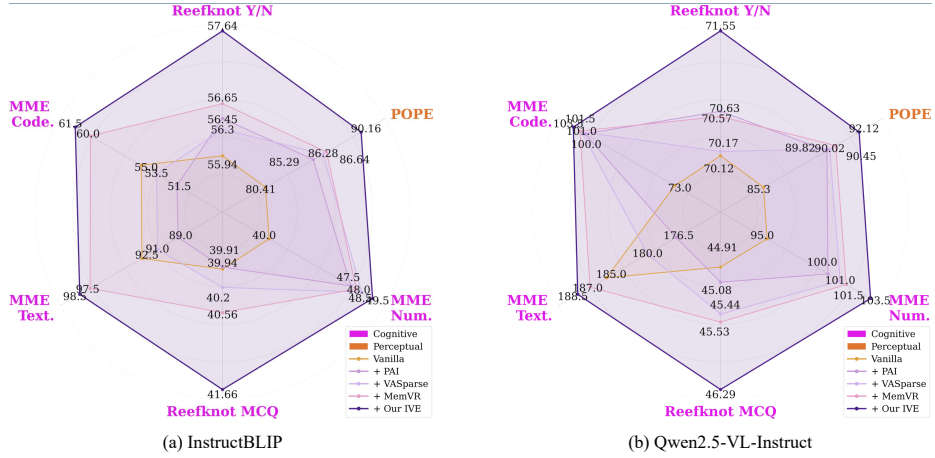


Fig. 7: Radar chart comparison of hallucination mitigation methods across multiple benchmarks under InstructBLIP [8] and Qwen2.5-VL-Instruct [2].

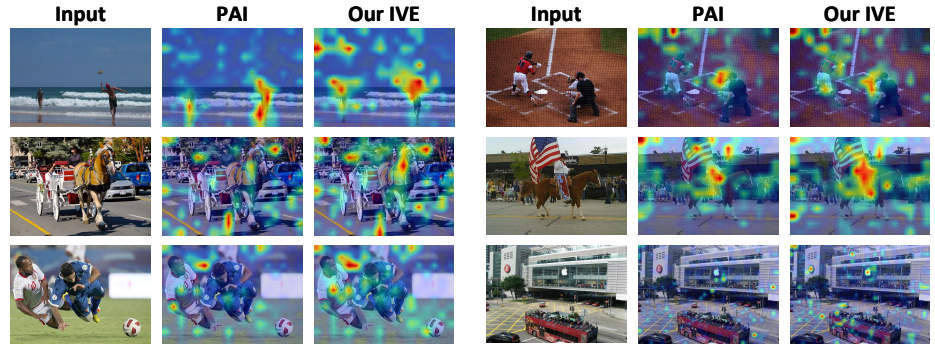


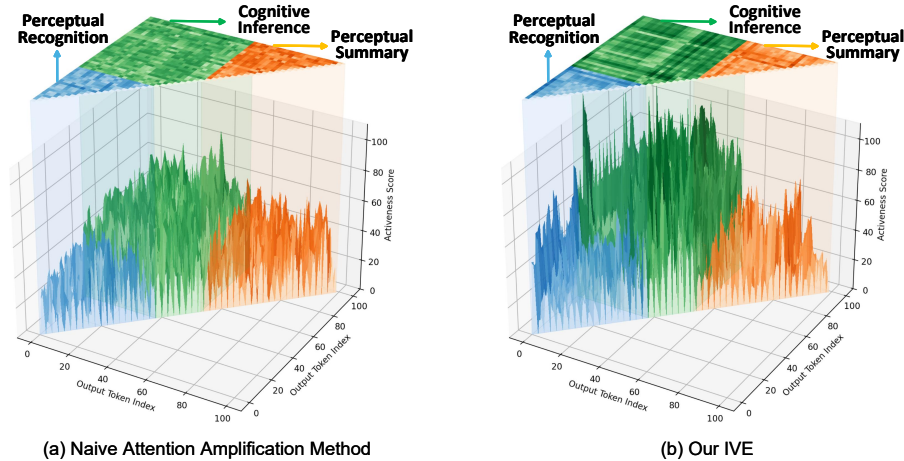
Fig. 8: Attention heatmap comparison between our IVE and the naive attention amplification method PAI [32].

Heatmap Comparison Between our IVE and PAI: Figure 8 presents a qualitative comparison of attention heatmaps generated by different methods. The visualization shows that responses produced by IVE distribute attention over multiple regions that are relationally relevant to the queried objects, indicating a more comprehensive visual grounding process. In contrast, the naive attention amplification method PAI [32] tends to concentrate attention within a limited spatial area, suggesting a narrower and less informative focus. This difference highlights that our IVE encourages broader cross-region evidence aggregation, which facilitates more reliable multimodal reasoning and helps reduce hallucination-prone responses.

Visual Activeness Comparison Between IVE and PAI: Figure 9 presents a comparison of visual attention dynamics between IVE and the naive visual at-

Table 7: Ablation study on key coefficients of IVE.

Param.	Model	Value	Reefknot [63]		POPE [25]		
			Perc.↓	Cogn.↓	R _{score} ↑	Acc↑	F1↑
γ	LLaVA-1.5 [30]	0.08	36.56	32.48	65.72	89.77	89.82
		0.09	35.79	31.88	66.40	90.63	90.68
		0.10	35.88	32.07	65.80	90.53	90.94
	InstructBLIP [8]	0.09	44.16	41.57	57.31	89.97	90.02
		0.10	43.75	40.60	57.64	90.20	90.16
		0.11	43.98	41.36	57.48	90.07	90.12
τ	LLaVA-1.5 [30]	2.95	36.72	32.44	65.67	89.63	89.68
		3.00	35.88	32.07	65.80	90.53	90.94
		3.05	35.93	32.10	65.73	90.27	90.32
	InstructBLIP [8]	3.00	43.75	40.60	57.64	90.20	90.16
		3.05	43.70	40.52	57.72	90.33	90.39
		3.10	43.88	40.99	57.61	90.10	90.11

**Fig. 9:** Visual activeness comparison between our IVE and the naive attention amplification method PAI [32].

tention amplification method PAI [32] during image captioning. The results show that PAI [32] consistently exhibits lower pairwise distances, indicating reduced semantic activeness in visual attention. In contrast, IVE maintains higher pairwise distances, suggesting more active and dynamic attention transitions across visual regions. This difference implies that naive attention amplification tends to exacerbate visual inertia, restricting attention to limited regions and hindering the capture of compositional semantics required for relational inference, whereas

IVE encourages more flexible attention shifts that better support multimodal inference and reduce cognitive hallucinations.

Ablation Study on Key Coefficients γ and τ : Table 7 reports the ablation results of the two key coefficients, γ and τ , in IVE, illustrating their influence on mitigating perceptual and cognitive hallucinations. For the coefficient γ , moderate values lead to the most stable improvements across both backbones. Specifically, when $\gamma = 0.09$ for LLaVA-1.5 [30] and $\gamma = 0.10$ for InstructBLIP [8], the models achieve the strongest overall performance on Reefknot [63] and POPE [25], demonstrating effective suppression of both perceptual and cognitive hallucinations. A similar trend can be observed for the temperature coefficient τ . When τ is set around 3.00–3.05, both models consistently obtain strong results across multiple evaluation metrics. Overall, across all tested configurations of γ and τ , IVE maintains stable improvements and consistently outperforms the state-of-the-art method MemVR [68], demonstrating the robustness and generalizability of the proposed approach.

9 Case Studies Across Different Datasets

To further illustrate the effectiveness of IVE, we present representative case studies across multiple widely used benchmark datasets.

Figure 10 ~ 17 present several representative examples where IVE successfully suppresses both perceptual and cognitive hallucinations. Compared with the baseline responses, the outputs generated by IVE demonstrate improved alignment with the visual content, capturing relevant objects, attributes, and inter-object relationships more reliably. These examples highlight that IVE can effectively guide the model to attend to semantically relevant visual regions and avoid generating unsupported or fabricated information.

Across multiple benchmarks, including Reefknot [63], MME [12], POPE [25], and MMBench [33], IVE consistently demonstrates strong capability in mitigating hallucinations under diverse evaluation settings. To ensure a fair and controlled comparison, all experiments are conducted using the LLaVA-1.5 model [30].

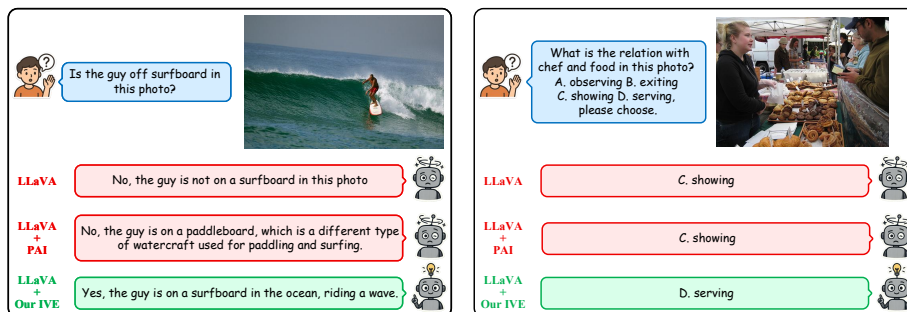


Fig. 10: An illustration of IVE mitigating cognitive hallucinations on Reefknot [63].

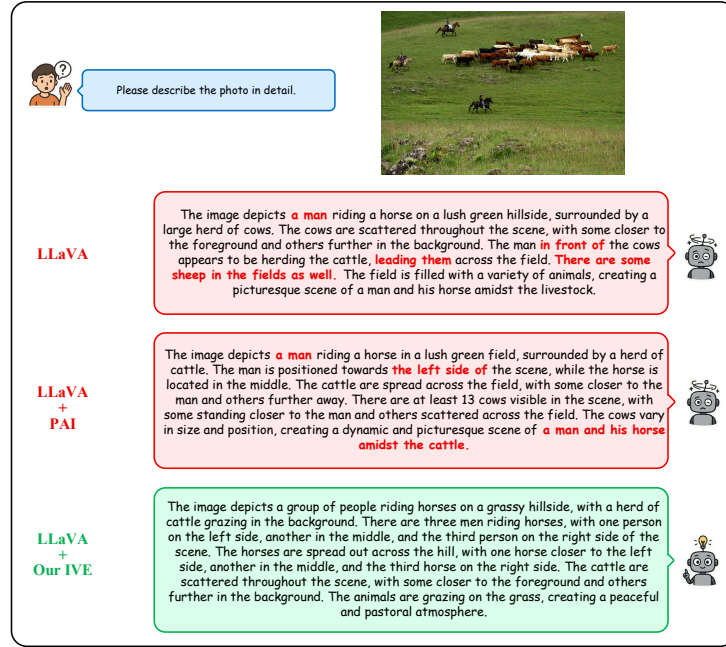


Fig. 11: An illustration of IVE mitigating cognitive hallucinations on Reefknot [63].



Fig. 12: An illustration of IVE mitigating cognitive hallucinations on Reefknot [63].

Please describe the photo in detail.

LLaVA

The image shows a baseball game in progress. A batter is swinging his bat as the ball approaches him. Nearby, a catcher wearing a **red baseball glove** is crouching **behind the batter**, ready to catch the ball if he misses. Several spectators **standing in the stands** can also be seen watching the game. Some of the players appear to be discussing the previous play, while others are preparing to run toward the bases.

LLaVA + PAI

The image captures a moment during a baseball game. A batter is swinging his bat, attempting to **hit the ball**. A nearby player wearing a professional catcher's glove stands behind him and is ready to **catch the ball** if the batter misses. Several other players are visible on the field, **standing and watching** the play. In the distance, a few teammates appear to be waiting near the bases. The atmosphere suggests that the game is at a tense and exciting moment.

LLaVA + Our IVE

The image captures an exciting moment during a baseball game. A baseball player is in the middle of swinging his bat, attempting to hit the ball. Another player, wearing a baseball glove, is positioned nearby, ready to catch the ball if the batter misses. There are several other people in the scene, including teammates and opponents. Some of them are standing in the background, while others are closer to the action. A baseball bat can be seen in the hands of the batter, and a baseball glove is visible in the hands of the player prepared to catch the ball.

Fig. 13: An illustration of IVE mitigating cognitive hallucinations on Reefknot [63].

Please describe the photo in detail.

LLaVA

The image shows four men gathered outdoors, working together to move a large white appliance. One of the men is **holding the metal refrigerator door** while another appears to be directing the group as they load the appliance into a **nearby truck**. Several bicycles are parked around them, and lush green plants with white and pink flowers line the background. A small dog sitting **beside the bicycles** can also be seen watching the activity.

LLaVA + PAI

The image shows four men standing together on a path, handling a large white appliance. One man **wearing a yellow work helmet** is holding the top of the appliance while another man stands behind him, **supervising the task**. Several bicycles are lying or parked nearby, and plants with flowers grow along the side of the path. The group appears to be carefully coordinating their movements while moving the heavy object.

LLaVA + Our IVE

The image shows four men gathered outdoors, working together to move a large white appliance, possibly a refrigerator or cabinet. One man is lifting the object while the others stand nearby assisting and guiding its movement. Several bicycles are parked around them, and green plants with white and pink flowers line the background, suggesting the scene takes place along a garden path or residential walkway.

Fig. 14: An illustration of IVE mitigating cognitive hallucinations on Reefknot [63].

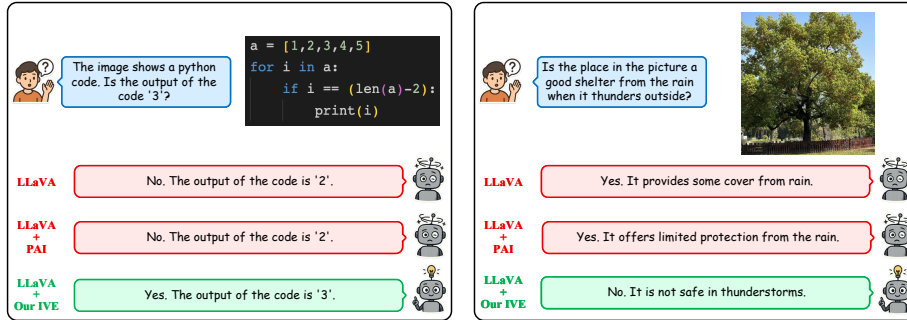


Fig. 15: An illustration of IVE mitigating cognitive hallucinations on MME [12].

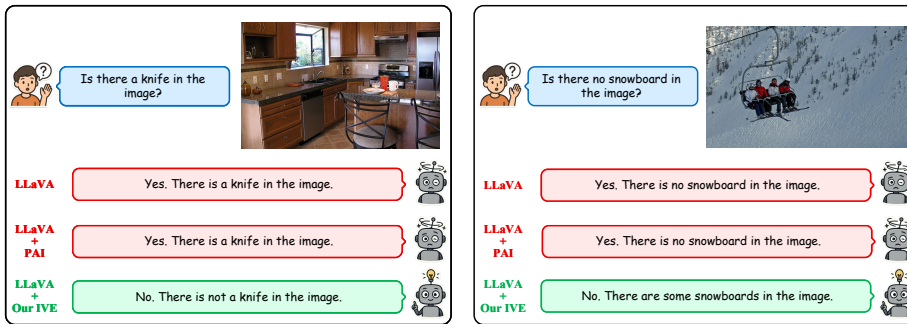


Fig. 16: An illustration of IVE mitigating perceptual hallucinations on POPE [25].

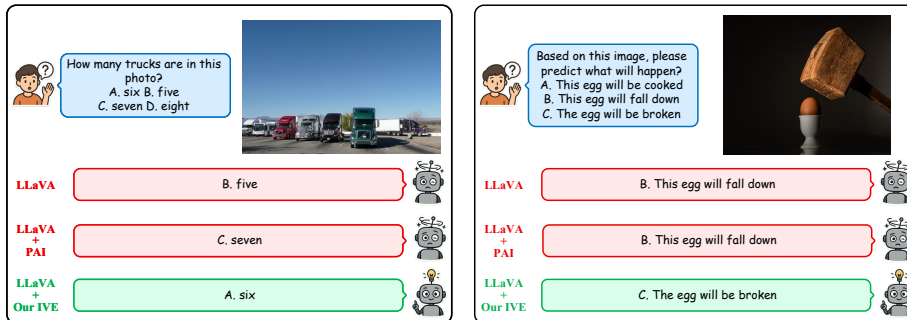


Fig. 17: An illustration of IVE mitigating cognitive hallucinations on MMBench [33].

References

1. Achiam, J., Adler, S., Agarwal, S., Ahmad, L., Akkaya, I., Aleman, F.L., Almeida, D., Altenschmidt, J., Altman, S., Anadkat, S., et al.: Gpt-4 technical report. arXiv preprint arXiv:2303.08774 (2023)
2. Bai, S., Chen, K., Liu, X., Wang, J., Ge, W., Song, S., Dang, K., Wang, P., Wang, S., Tang, J., et al.: Qwen2. 5-vl technical report. arXiv preprint arXiv:2502.13923 (2025)
3. Chen, L., Sinavski, O., Hünermann, J., Karnsund, A., Willmott, A.J., Birch, D., Maund, D., Shotton, J.: Driving with llms: Fusing object-level vector modality for explainable autonomous driving. In: ICRA. pp. 14093–14100 (2024)
4. Chen, Z., Zhao, Z., Luo, H., Yao, H., Li, B., Zhou, J.: Halc: Object hallucination reduction via adaptive focal-contrast decoding. In: ICML. pp. 7824–7846 (2024)
5. Cherti, M., Beaumont, R., Wightman, R., Wortsman, M., Ilharco, G., Gordon, C., Schuhmann, C., Schmidt, L., Jitsev, J.: Reproducible scaling laws for contrastive language-image learning. In: CVPR. pp. 2818–2829 (2023)
6. Chiang, W.L., Li, Z., Lin, Z., Sheng, Y., Wu, Z., Zhang, H., Zheng, L., Zhuang, S., Zhuang, Y., Gonzalez, J.E., et al.: Vicuna: An open-source chatbot impressing gpt-4 with 90%* chatgpt quality. See <https://vicuna.lmsys.org> (accessed 14 April 2023) **2**(3), 6 (2023)
7. Chuang, Y.S., Xie, Y., Luo, H., Kim, Y., Glass, J., He, P.: Dola: Decoding by contrasting layers improves factuality in large language models. In: ICLR. pp. 54158–54183 (2024)
8. Dai, W., Li, J., Li, D., Tiong, A., Zhao, J., Wang, W., Li, B., Fung, P.N., Hoi, S.: Instructblip: Towards general-purpose vision-language models with instruction tuning. In: NeurIPS. vol. 36, pp. 49250–49267 (2023)
9. Dai, W., Liu, Z., Ji, Z., Su, D., Fung, P.: Plausible may not be faithful: Probing object hallucination in vision-language pre-training. In: EACL. pp. 2136–2148 (2023)
10. Devlin, J., Chang, M.W., Lee, K., Toutanova, K.: Bert: Pre-training of deep bidirectional transformers for language understanding. In: NAACL. pp. 4171–4186 (2019)
11. Ding, Y., Zhu, X., Xia, T., Wu, J., Chen, X., Liu, Q., Wang, L.: D² hscore: Reasoning-aware hallucination detection via semantic breadth and depth analysis in llms. arXiv preprint arXiv:2509.11569 (2025)
12. Fu, C., Chen, P., Shen, Y., Qin, Y., Zhang, M., Lin, X., Yang, J., Zheng, X., Li, K., Sun, X., et al.: Mme: A comprehensive evaluation benchmark for multimodal large language models. In: NeurIPS (2025)
13. GLM, T., Zeng, A., Xu, B., Wang, B., Zhang, C., Yin, D., Zhang, D., Rojas, D., Feng, G., Zhao, H., et al.: Chatglm: A family of large language models from glm-130b to glm-4 all tools. arXiv preprint arXiv:2406.12793 (2024)
14. Guan, T., Liu, F., Wu, X., Xian, R., Li, Z., Liu, X., Wang, X., Chen, L., Huang, F., Yacoob, Y., et al.: Hallusionbench: an advanced diagnostic suite for entangled language hallucination and visual illusion in large vision-language models. In: CVPR. pp. 14375–14385 (2024)
15. Gunjal, A., Yin, J., Bas, E.: Detecting and preventing hallucinations in large vision language models. In: AAAI. vol. 38, pp. 18135–18143 (2024)
16. Hu, M., Pan, S., Li, Y., Yang, X.: Advancing medical imaging with language models: A journey from n-grams to chatgpt. arXiv preprint arXiv:2304.04920 (2023)

17. Huang, Q., Dong, X., Zhang, P., Wang, B., He, C., Wang, J., Lin, D., Zhang, W., Yu, N.: Opera: Alleviating hallucination in multi-modal large language models via over-trust penalty and retrospection-allocation. In: CVPR. pp. 13418–13427 (2024)
18. Jiang, C., Xu, H., Dong, M., Chen, J., Ye, W., Yan, M., Ye, Q., Zhang, J., Huang, F., Zhang, S.: Hallucination augmented contrastive learning for multimodal large language model. In: CVPR. pp. 27036–27046 (2024)
19. Jung, M., Lee, S., Kim, E., Yoon, S.: Visual attention never fades: Selective progressive attention recalibration for detailed image captioning in multimodal large language models. In: ICML (2025)
20. Kim, M., Kim, M., Bae, J., Choi, S., Kim, S., Chang, B.: Exploiting semantic reconstruction to mitigate hallucinations in vision-language models. In: ECCV. pp. 236–252 (2024)
21. Leng, S., Zhang, H., Chen, G., Li, X., Lu, S., Miao, C., Bing, L.: Mitigating object hallucinations in large vision-language models through visual contrastive decoding. In: CVPR. pp. 13872–13882 (2024)
22. Li, J., Li, D., Savarese, S., Hoi, S.: Blip-2: Bootstrapping language-image pre-training with frozen image encoders and large language models. In: ICML. pp. 19730–19742 (2023)
23. Li, K., Patel, O., Viégas, F., Pfister, H., Wattenberg, M.: Inference-time intervention: Eliciting truthful answers from a language model. In: NeurIPS. vol. 36, pp. 41451–41530 (2023)
24. Li, X.L., Holtzman, A., Fried, D., Liang, P., Eisner, J., Hashimoto, T., Zettlemoyer, L., Lewis, M.: Contrastive decoding: Open-ended text generation as optimization. In: ACL. p. 12286–12312 (2023)
25. Li, Y., Du, Y., Zhou, K., Wang, J., Zhao, W.X., Wen, J.R.: Evaluating object hallucination in large vision-language models. In: EMNLP (2023)
26. Lin, T.Y., Maire, M., Belongie, S., Hays, J., Perona, P., Ramanan, D., Dollár, P., Zitnick, C.L.: Microsoft coco: Common objects in context. In: ECCV. pp. 740–755 (2014)
27. Liu, A., Feng, B., Xue, B., Wang, B., Wu, B., Lu, C., Zhao, C., Deng, C., Zhang, C., Ruan, C., et al.: Deepseek-v3 technical report. arXiv preprint arXiv:2412.19437 (2024)
28. Liu, F., Lin, K., Li, L., Wang, J., Yacoob, Y., Wang, L.: Aligning large multi-modal model with robust instruction tuning. In: ICLR. pp. 57689–57733 (2024)
29. Liu, H., Zhu, Y., Kato, K., Kondo, I., Aoyama, T., Hasegawa, Y.: Llm-based human-robot collaboration framework for manipulation tasks. arXiv preprint arXiv:2308.14972 (2023)
30. Liu, H., Li, C., Li, Y., Lee, Y.J.: Improved baselines with visual instruction tuning. In: CVPR. pp. 26296–26306 (2024)
31. Liu, H., Li, C., Wu, Q., Lee, Y.J.: Visual instruction tuning. In: NeurIPS. vol. 36, pp. 34892–34916 (2024)
32. Liu, S., Zheng, K., Chen, W.: Paying more attention to image: A training-free method for alleviating hallucination in vlms. In: ECCV. pp. 125–140 (2024)
33. Liu, Y., Duan, H., Zhang, Y., Li, B., Zhang, S., Zhao, W., Yuan, Y., Wang, J., He, C., Liu, Z., et al.: Mmbench: Is your multi-modal model an all-around player? In: ECCV. pp. 216–233 (2024)
34. Mai, J., Chen, J., Li, B., Qian, G., Elhoseiny, M., Ghanem, B.: Llm as a robotic brain: Unifying egocentric memory and control. arXiv preprint arXiv:2304.09349 (2023)

35. Radford, A., Kim, J.W., Hallacy, C., Ramesh, A., Goh, G., Agarwal, S., Sastry, G., Askell, A., Mishkin, P., Clark, J., et al.: Learning transferable visual models from natural language supervision. In: ICML. pp. 8748–8763 (2021)
36. Ren, J., Zhao, Y., Vu, T., Liu, P.J., Lakshminarayanan, B.: Self-evaluation improves selective generation in large language models. In: NeurIPS Workshop (2023)
37. Rohrbach, A., Hendricks, L.A., Burns, K., Darrell, T., Saenko, K.: Object hallucination in image captioning. In: EMNLP (2018)
38. Su, W., Wang, C., Ai, Q., Hu, Y., Wu, Z., Zhou, Y., Liu, Y.: Unsupervised real-time hallucination detection based on the internal states of large language models. In: ACL. pp. 14379–14391 (2025)
39. Sun, Z., Shen, S., Cao, S., Liu, H., Li, C., Shen, Y., Gan, C., Gui, L., Wang, Y.X., Yang, Y., et al.: Aligning large multimodal models with factually augmented rlhf. In: ACL. pp. 13088–13110 (2024)
40. Taori, R., Gulrajani, I., Zhang, T., Dubois, Y., Li, X., Guestrin, C., Liang, P., Hashimoto, T.B.: Stanford alpaca: An instruction-following llama model (2023)
41. Tian, K., Mitchell, E., Zhou, A., Sharma, A., Rafailov, R., Yao, H., Finn, C., Manning, C.D.: Just ask for calibration: Strategies for eliciting calibrated confidence scores from language models fine-tuned with human feedback. In: ACL. p. 5433–5442 (2023)
42. Touvron, H., Lavril, T., Izacard, G., Martinet, X., Lachaux, M.A., Lacroix, T., Rozière, B., Goyal, N., Hambro, E., Azhar, F., et al.: Llama: Open and efficient foundation language models. arXiv preprint arXiv:2302.13971 (2023)
43. Touvron, H., Martin, L., Stone, K., Albert, P., Almahairi, A., Babaei, Y., Bashlykov, N., Batra, S., Bhargava, P., Bhosale, S., et al.: Llama 2: Open foundation and fine-tuned chat models. arXiv preprint arXiv:2307.09288 (2023)
44. Vaswani, A., Shazeer, N., Parmar, N., Uszkoreit, J., Jones, L., Gomez, A.N., Kaiser, Ł., Polosukhin, I.: Attention is all you need. *NeurIPS* **30** (2017)
45. Wang, C., Chen, X., Zhang, N., Tian, B., Xu, H., Deng, S., Chen, H.: Mllm can see? dynamic correction decoding for hallucination mitigation. In: ICLR. pp. 13712–13736 (2025)
46. Wang, S., Zhao, Z., Ouyang, X., Liu, T., Wang, Q., Shen, D.: Interactive computer-aided diagnosis on medical image using large language models. *Communications Engineering* **3**(1), 133 (2024)
47. Wang, X., Pan, J., Ding, L., Biemann, C.: Mitigating hallucinations in large vision-language models with instruction contrastive decoding. In: ACL. p. 15840–15853 (2024)
48. Wolf, T., Debut, L., Sanh, V., Chaumond, J., Delangue, C., Moi, A., Cistac, P., Rault, T., Louf, R., Funtowicz, M., et al.: Huggingface’s transformers: State-of-the-art natural language processing. arXiv preprint arXiv:1910.03771 (2019)
49. Wu, Z., Wang, Z., Xu, X., Lu, J., Yan, H.: Embodied task planning with large language models. arXiv preprint arXiv:2307.01848 (2023)
50. Xie, Y., Zhu, Z., Zhuang, X., Liang, L., Wang, Z., Zou, Y.: Gpa: Global and prototype alignment for audio-text retrieval. In: Proc. Interspeech. pp. 5078–5082 (2024)
51. Yin, H., Si, G., Wang, Z.: ClearSight: Visual signal enhancement for object hallucination mitigation in multimodal large language models. In: CVPR. pp. 14625–14634 (2025)
52. Yin, Y., Xie, Y., Yang, W., Yang, D., Ru, J., Zhuang, X., Liang, L., Zou, Y.: Atri: Mitigating multilingual audio text retrieval inconsistencies by reducing data distribution errors. In: ACL. pp. 5491–5504 (2025)

53. Yu, Q., Li, J., Wei, L., Pang, L., Ye, W., Qin, B., Tang, S., Tian, Q., Zhuang, Y.: Hallucidoctor: Mitigating hallucinatory toxicity in visual instruction data. In: CVPR. pp. 12944–12953 (2024)
54. Yu, T., Yao, Y., Zhang, H., He, T., Han, Y., Cui, G., Hu, J., Liu, Z., Zheng, H.T., Sun, M., et al.: Rllhf-v: Towards trustworthy mllms via behavior alignment from fine-grained correctional human feedback. In: CVPR. pp. 13807–13816 (2024)
55. Yu, X., Xu, C., Zhang, G., He, Y., Chen, Z., Xue, Z., Zhang, J., Liao, Y., Hu, X., Jiang, Y.G., et al.: Visual multi-agent system: Mitigating hallucination snowballing via visual flow. arXiv preprint arXiv:2509.21789 (2025)
56. Yuan, F., Qin, C., Xu, X., Li, P.: Helpd: Mitigating hallucination of lvlms by hierarchical feedback learning with vision-enhanced penalty decoding. In: EMNLP. pp. 1768–1785 (2024)
57. Yue, Z., Zhang, L., Jin, Q.: Less is more: Mitigating multimodal hallucination from an eos decision perspective. In: ACL. pp. 11766–11781 (2024)
58. Zhai, X., Mustafa, B., Kolesnikov, A., Beyer, L.: Sigmoid loss for language image pre-training. In: CVPR. pp. 11975–11986 (2023)
59. Zhang, Y., Cui, L., Shi, S., et al.: Alleviating hallucinations of large language models through induced hallucinations. In: NAACL. pp. 8218–8232 (2025)
60. Zhang, Y., Li, Y., Cui, L., Cai, D., Liu, L., Fu, T., Huang, X., Zhao, E., Zhang, Y., Chen, Y., et al.: Siren’s song in the ai ocean: A survey on hallucination in large language models. Computational Linguistics pp. 1–46 (2025)
61. Zhao, Y., Li, K., Cheng, Z., Qiao, P., Zheng, X., Ji, R., Liu, C., Yuan, L., Chen, J.: Graco: Granularity-controllable interactive segmentation. In: CVPR. pp. 3501–3510 (2024)
62. Zhao, Y., Lv, W., Xu, S., Wei, J., Wang, G., Dang, Q., Liu, Y., Chen, J.: Detrs beat yolos on real-time object detection. In: CVPR. pp. 16965–16974 (2024)
63. Zheng, K., Chen, J., Yan, Y., Zou, X., Hu, X.: Reefknot: A comprehensive benchmark for relation hallucination evaluation, analysis and mitigation in multimodal large language models. In: ACL. pp. 6193–6212 (2024)
64. Zheng, L., Chiang, W.L., Sheng, Y., Zhuang, S., Wu, Z., Zhuang, Y., Lin, Z., Li, Z., Li, D., Xing, E., et al.: Judging llm-as-a-judge with mt-bench and chatbot arena. In: NeurIPS. vol. 36, pp. 46595–46623 (2023)
65. Zhu, D., Chen, J., Shen, X., Li, X., Elhoseiny, M.: Minigpt-4: Enhancing vision-language understanding with advanced large language models. In: ICLR. pp. 18378–18394 (2024)
66. Zhuang, X., Cheng, X., Zhu, Z., Chen, Z., Li, H., Zou, Y.: Towards multimodal-augmented pre-trained language models via self-balanced expectation-maximization iteration. In: ACM MM (2024)
67. Zhuang, X., Zhu, Z., Xie, Y., Liang, L., Zou, Y.: Vasparse: Towards efficient visual hallucination mitigation via visual-aware token sparsification. In: CVPR. pp. 4189–4199 (2025)
68. Zou, X., Wang, Y., Yan, Y., Lyu, Y., Zheng, K., Huang, S., Chen, J., Jiang, P., Liu, J., Tang, C., et al.: Look twice before you answer: Memory-space visual retracing for hallucination mitigation in multimodal large language models. In: ICML (2025)